

Commercial Accelerometers for Vibration Sensing at mK Temperatures in Dry Dilution Refrigerators

A. D'Addabbo^a S. D'Eramo^{a,b} S.H. Fu^a M.T. Hurst^c T. O'Donnell^d S. Pettii^{1e} V. Sharma^c P. T. Surukuchi^{2c} A. Torres^d C. Wengappuliarachchige^d K. J. Vetter^f N. Brace^d

^a*INFN – Laboratori Nazionali del Gran Sasso, Assergi (L'Aquila) I-67100, Italy*

^b*DIIIE, Università degli Studi dell'Aquila, Monteluco di Roio, L'Aquila 67100, Italy*

^c*Department of Physics and Astronomy, University of Pittsburgh, Pittsburgh, PA 15260, USA*

^d*Center for Neutrino Physics, Virginia Polytechnic Institute and State University, Blacksburg, Virginia 24061, USA*

^e*INFN – TIFPA, c/o Dip. di Fisica Università di Trento, Povo (TN), I-38123, Italy*

^f*Massachusetts Institute of Technology, Cambridge, MA 02139, USA*

E-mail: surukuchi@pitt.edu

ABSTRACT: This article presents an evaluation of off-the-shelf commercial accelerometers at the mixing chamber stage of a cryogen-free dilution refrigerator at temperatures down to 8 mK. In addition, we present results of radioassay of accelerometer samples using a high purity germanium detector counting setup. Cryogen-free dilution refrigerators using pulse-tube cryocoolers (PTs) — due to recent advances in their cooling capacity, long-term stability, and operational costs — have become ubiquitous tools in a wide range of fields ranging from experimental particle physics to quantum information sciences. However, vibrations induced by PTs can negatively impact the experimental payload in these applications. This work demonstrates that commercially available accelerometers can not only measure vibrations at millikelvin cryogenic temperatures but also pave the way for continuous, *in situ*, real-time vibration monitoring of dry dilution refrigerators.

KEYWORDS: Cryogenic detectors, Cryocoolers, Vibration analysis, Instrumental noise

¹currently at Dip. di Fisica Università di Torino, Torino (TO) I-10125, Italy

²Corresponding author.

Contents

1	Introduction and Motivation	1
2	Experimental Setup	2
3	Vibration Measurement Results	5
4	Radioassay Results	8
5	Discussion	10

1 Introduction and Motivation

Cryogenic calorimetry is among the most sensitive technologies for a wide range of fundamental physics applications, including neutrinoless double beta decay searches $0\nu\beta\beta$ [1–4], coherent elastic neutrino–nucleus scattering [5, 6], direct neutrino mass measurements [7, 8], and dark matter experiments [9–11]. These capabilities rely on stable operation of large detector volumes at millikelvin (mK) temperatures. Dilution refrigerators operate on the principle of ^3He - ^4He mixing [12] and can be designed to reliably cool large mass payloads down to below 10mK [13].

Wet dilution refrigerators, employing liquid helium for pre-cooling, are well-established and have been used extensively for decades. Dry dilution refrigerators (DDR), using mechanical cryogen-free pre-cooling, are increasingly replacing wet refrigerators due to their growing cooling powers, long-term operational stability [14], and reduced reliance on volatile helium supplies.

The absence of moving parts at the cold stage makes PTs a lower-vibration alternative to other cryocooler technologies such as GM tubes for pre-cooling DDRs, and have been widely adopted in various applications, ranging from fundamental physics to the rapidly expanding field of quantum computing [15]. However, pressure wave-induced vibrations can still propagate down to the experimental volume of the DDRs, thereby limiting their capabilities. In cryogenic calorimeters, these vibrations manifest as reduced energy resolution [16], elevated detector thresholds, and reduced efficiency [17]. Furthermore, they present a growing challenge for the usage of DDRs in quantum sensing and quantum computing applications [18].

To address these limitations, vibration reduction through passive decoupling of the stages of DDRs has emerged as an important area of research. Approaches, such as springs [19–24], bellows [25], and foam [16], have been explored with varying success. The performance of the decoupling systems can be evaluated by deploying vibration sensors, such as accelerometers, on their room temperature flange (300 K plate) [25]. But this approach assumes vibration characteristics are consistent between the 300 K plate and the experimental volume, which is not universally applicable. Geophones have also been employed [26–30] for vibration sensing across room-temperature and cryogenic environments, down to 3 K. However, low-frequency geophones are typically large

in volume, posing challenges for space-constrained, thermally-restrictive, or radiation-sensitive applications. Therefore, it is desirable to deploy low-mass vibration sensors, as witness channels, close to the experimental volume.

Furthermore, as experiments become increasingly sensitive to low vibration levels, not only from PTs but also other ambient sources such as microseisms [17], the need for continuous vibration detection and monitoring with high sensitivity is increasingly critical. A particularly compelling example is the CUORE experiment, in which vibrations are measured using several witness channels — including accelerometers, seismometers, and microphones — installed around the cryostat. These measurements are then correlated to effectively reduce noise [31] in the calorimeters suspended from the mixing chamber (MC) plate. To further improve sensitivity, CUORE and other similar cryogenic experiments would benefit from continuous vibration monitoring, with witness channels placed directly on the MC plate or in other locations closer to the experimental volume.

In this article, we present a vibration monitoring setup using commercially available, cost-effective accelerometers that can be deployed at the MC stage of a DDR. Using this setup, we monitored PT-induced vibrations at a broad range of stable temperatures, ranging from 8 mK upto 1 K, including an extended measurement at 8 mK. We discuss the experimental setup in Section 2, including details on the DDR, selection of accelerometers and the data acquisition systems for temperature and accelerometer measurements. The results of the vibration measurements are presented in Section 3. Section 4 covers the setup and results of the radioassay on the accelerometers. In Section 5, we conclude with a discussion of the findings, potential improvements, and future prospects.

2 Experimental Setup

All cryogenic vibration measurements in this study employed a triaxial configuration of three Endevco 2271A piezoelectric accelerometers [32] (weighing 27 g) mounted on the MC plate via a custom-machined oxygen-free electronic (OFE) grade copper mounting block. The accelerometer outputs were fed into and amplified by a four-channel PCB Piezotronics 482C64 conditioner [33], which features selectable charge-to-voltage conversion settings (0.1 mV/pC, 1 mV/pC, and 10 mV/pC), along with an additional incremental voltage gain setting between x0.1 and x200. The 2271A has a charge sensitivity of 11.5 pC/g, specified over 1–8000 Hz frequency range and rated for operation down to 4K. All data were acquired with the conditioner configured at a charge-to-voltage conversion factor of 10 mV/pC and a voltage gain of 42.74, resulting in a system gain of 4915 mV/g. The overall gain was selected to prevent saturating the signal conditioner’s dynamic range during typical cryostat vibration acquisition conditions. The gains of all three 2271A accelerometers were set identically to allow for relative comparisons between vibrations in each direction of the triaxial setup.

A separate triaxial setup with three PCB Piezotronics 393B31 accelerometers [34] was used as a control to assess relative variations in the vibrational environment, with the accelerometers mounted on an aluminum block on the 300K plate in close proximity to the pulse tube cryocoolers. A four-channel PCB Piezotronics 482C15 conditioner [35], with selectable gain settings of x1, x10, and x100, was used to amplify the signals from the accelerometers. All data were acquired

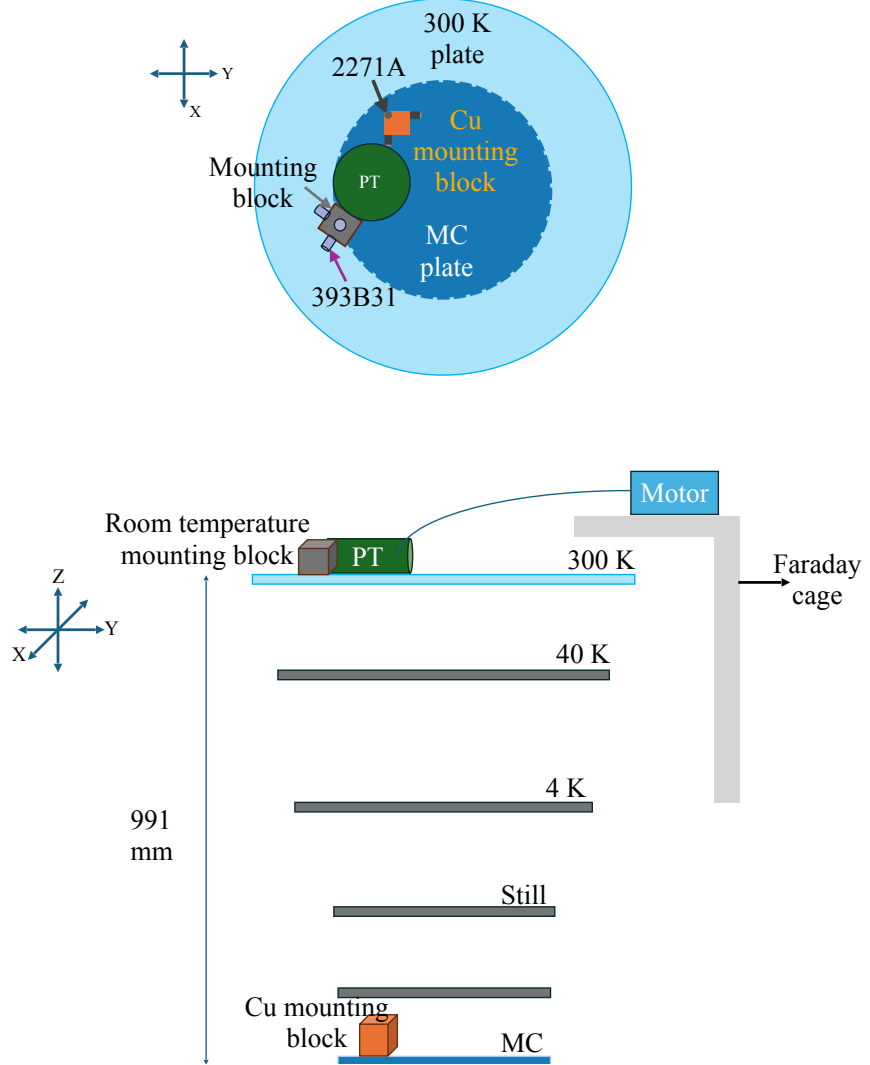


Figure 1. (Top): Schematic of the cryostat as seen from the top showing the placement of the mounting blocks. Also shown are their placements relative to the PT head. The strongest impulse from PTs is approximately along the Y-axis on the schematic. Only the 300K and the MC plate are shown for the sake of clarity. (Bottom): Lateral view of the measurement setup.

with the conditioner gain setting configured at x1, which when combined with the rated sensitivity of 393B31 at 10 V/g (0.1–200 Hz), resulted in a total gain of 10000 mV/g.

The accelerometer-conditioner combinations for both the room temperature and cryogenic setups were chosen to maximize sensitivity at low frequencies (~ 1 Hz). Since we did not perform an absolute calibration against a known vibration source, all accelerometer data are reported in arbitrary units and are intended for comparison only. figure 1 shows the placement of both sets of accelerometers, positioned so that one of the accelerometers approximately aligns with the direction of the strongest PT impulses.

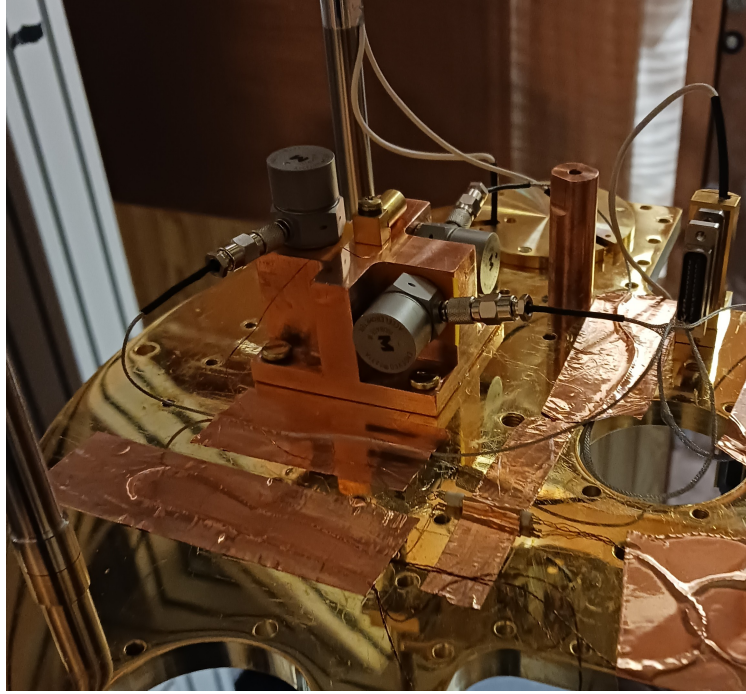


Figure 2. Photograph of the mounting block with all three 2271A accelerometers mounted in a triaxial setup, as used for all the measurements. Also visible on top of the mounting block is the RuOx thermometer.

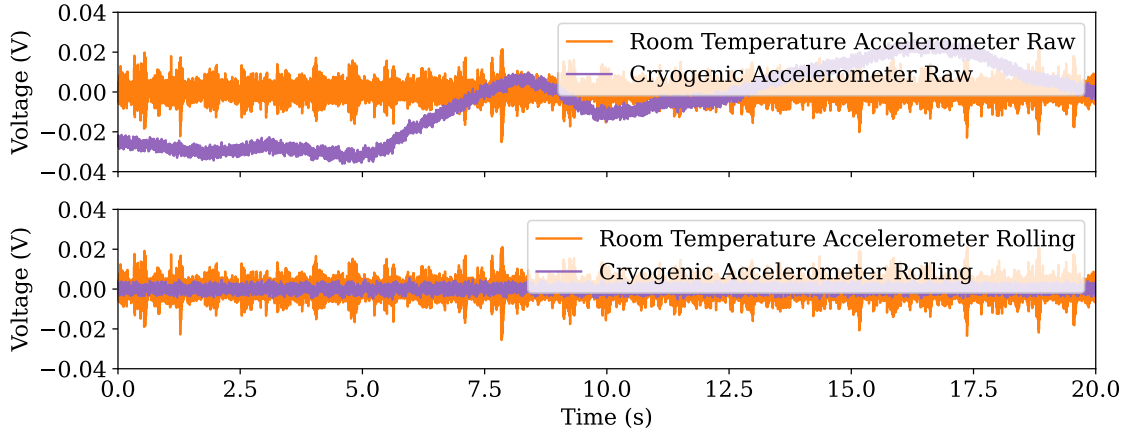


Figure 3. (Top): Raw voltage time series data of a 393B31 accelerometer and a 2271A accelerometer, clearly showing a drift in the baseline of the 2271A accelerometer. (Bottom): The same data smoothed by applying a 0.5 s rolling average subtraction. The baseline voltage drift was corrected for the 2271A accelerometers, while no noticeable variations were observed in the 393B31 accelerometers.

The signals from all six channels, routed through the respective conditioners, are fed to National Instruments (NI) DAQ 9230 module [36] integrated with NI cDAQ 9178 chassis [37] for digitization. 9230 is a three-channel DAQ with 24-bit ADC resolution and a maximum sampling rate of 12.8 kS/s. All data were acquired at a sampling rate of 1 kS/s. An NI LabVIEW program was used for data acquisition, segmenting the data into 10-second intervals and recording them to disk. An

additional offline preprocessing step was used to merge the 10-second segments into a single long time series of the required duration. To address slow drifts (\sim s-scale) observed in the 2271A data, we applied a 0.5 s rolling average subtraction, as shown in figure 3, to the entire time series for all datasets.

The measurements were carried out at a cryogenic facility located in Robeson Hall, Virginia Tech. The facility includes a Bluefors LD400 DDR, equipped with a Cryomech PT415 PT with a remote motor. A nearby NESLAB HX750 air-cooled chiller cools the PT compressor and DDR gas handling system. Vibrations from the gas handling system are decoupled from the cryostat by a bellows T-damper in the still pumping line. To reduce electromagnetic interference, the refrigerator is housed inside a Faraday room. The PT remote motor is mounted outside the Faraday room on an aluminum frame decoupled from the Faraday room, just above the room ceiling. It is coupled via a \sim 30 cm flex line to the PT cold head, which is mounted using a Bluefors-provided bellows to the the 300 K plate of the cryostat. The 40K and 4K stages of the PT are thermally coupled to the 40K and 4K stages of the refrigerator via flexible copper braids.

The temperatures of the MC plate and the mounting block were monitored using two ruthenium oxide (RuO_x) Lakeshore RX-102B thermometers. These measurements were recorded using a Lakeshore 372 AC resistance bridge. All temperature measurements in this study, unless explicitly stated, correspond to the thermometer attached to the MC plate. The MC plate was also instrumented with a $120\ \Omega$ resistive heater to adjust the temperatures to desired values by applying configurable currents.

3 Vibration Measurement Results

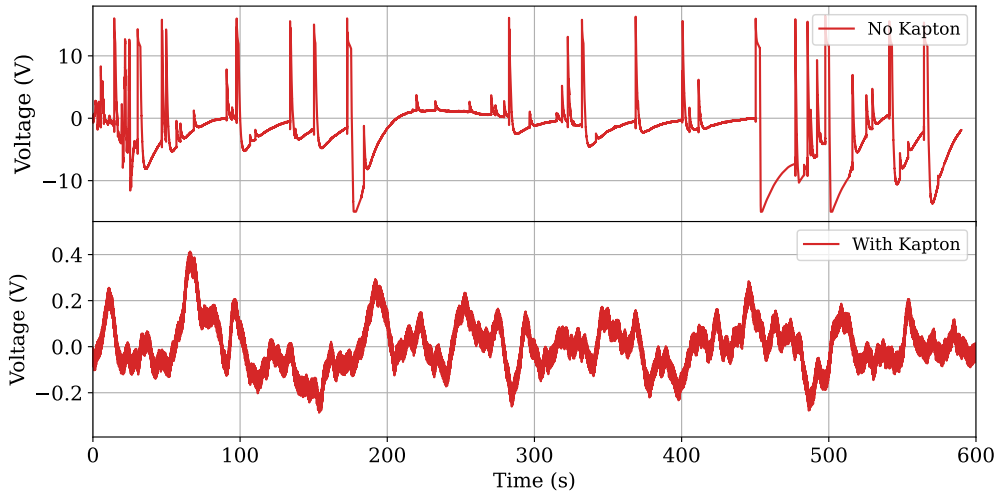


Figure 4. (Top): Time series of 2271A accelerometer voltage on the MC plate with no Kapton tape electrical insulation. (Bottom): Time series of 2271A accelerometer voltage on the MC plate with Kapton tape on brass screws and the interface between mounting block and accelerometer. Notice the difference in voltage scales between the two figures.

The data-taking began with the proprietary Endevco 3090C cables provided with the cryogenic

accelerometers. The 10 ft long cables were thermalized at each stage by compressing a \sim 15 cm segment between copper plates thermally connected to the stage. These cables were connected to vacuum feedthroughs at the 300K plate, the other end of which were connected to the conditioners via BNC cables. The cables carrying the signal from the feedthroughs to the DAQ were affixed to the exterior of the walls of the Faraday cage to minimize the effect of the cables' vibration on the accelerometer output. We found that the minimum temperature reached by the MC plate in this configuration was 60 mK, compared to 8 mK in the absence of load. We attribute the additional heat load to the Endevco 3090C cables [38] which were rated for a minimum temperature of 4 K.

We initially observed spurious electrical discharges manifesting as high voltage spikes. To electrically isolate the body of the accelerometers from the copper mounting block, we used a thin layer of Kapton film between them. Further, the body of the brass screws that were to secure the accelerometers to the mounting block, were electrically isolated using Kapton washers and sleeves. These steps helped to diminish the spikes as shown in figure 4.

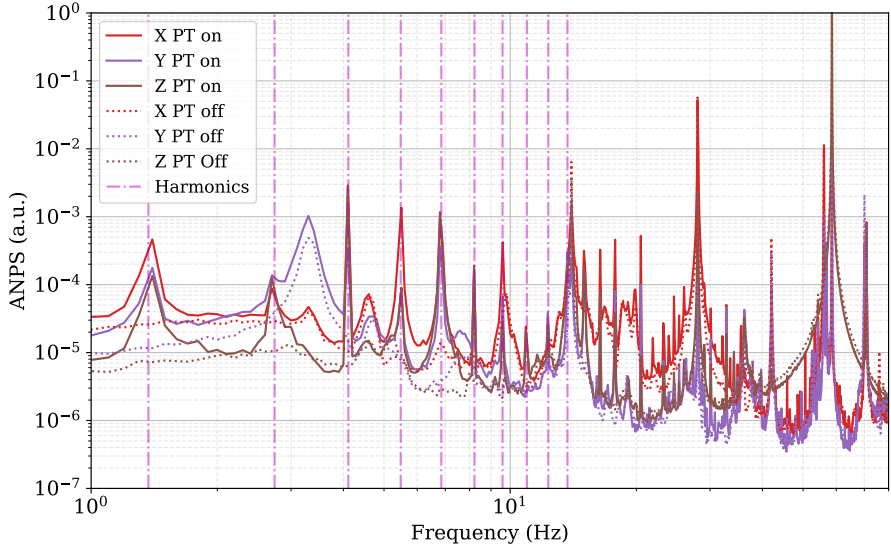


Figure 5. ANPS of 2271A accelerometers, after MC plate stabilized at 8 mK, when the PT was on (solid lines) and turned off (dotted lines). Also shown are the 1.4 Hz base frequency of the PT and its next nine harmonics clearly illustrating the sensitivity of the accelerometers to vibrations.

To minimize the heat load at the base temperature of the DDR, we switched the Endevco cables with three-channel custom breakout cable, consisting of short (\sim 20 cm) segments, of low-mass shielded NbTi cable (CMR 02-32-052) to couple each accelerometer output to the permanently installed low-mass readout wiring in the refrigerator. The permanently installed wiring terminates at an MDM25 connector on the MC plate and is composed of twisted pair NbTi from the MC plate to the 4K plate and twisted pair copper to the 300K flange. One end of each channel was soldered to a Pasternack PE44353 microdot connector to couple it to an accelerometer and the other end was soldered to the MDM connector. This change enabled the MC plate to achieve the cryostat's no-load base temperature of 8 mK. The corresponding mounting block temperature stabilized at

15.2 mK. Through the rest of the paper, we quote the temperature as measured on the MC plate.

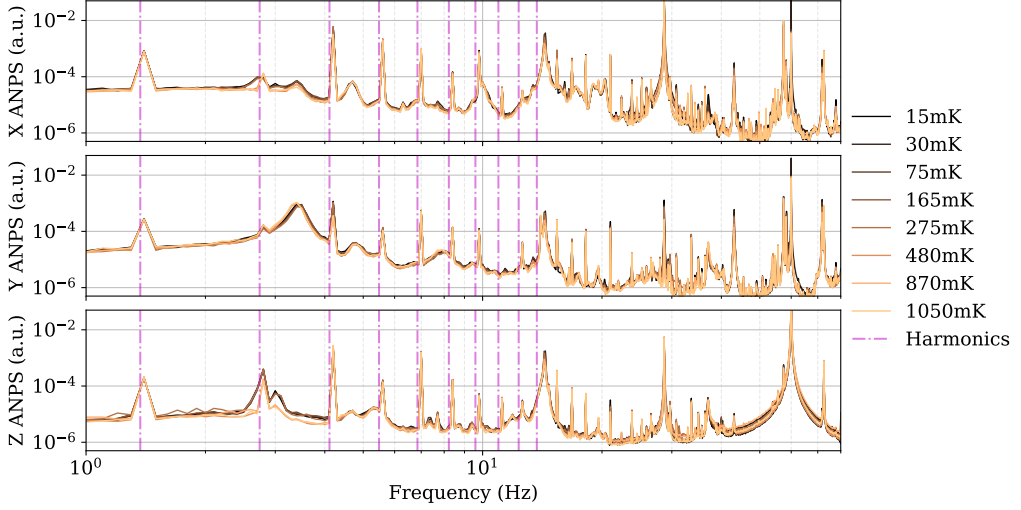


Figure 6. Stability of the response of all three 2271A accelerometers over MC plate temperatures ranging from 15 mK to 1050 mK, rounded to the nearest 5 mK. Each ANPS was generated using one hour of data.

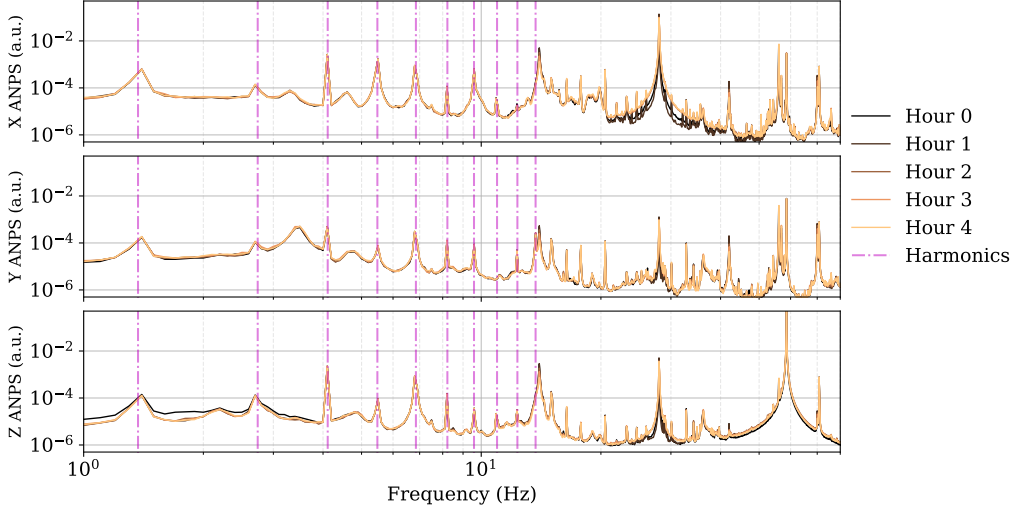


Figure 7. Stability of the response of the 2271A accelerometers over five consecutive hours, separated into 1 hour segments. Average temperature of MC Plate during this data period was 8.0 mK.

Data from all six channels were processed by applying a rolling average subtraction, segmenting the data into 10 s windows, applying fast Fourier transforms (FFTs) to compute the power spectral density (PSD), and averaging the results to obtain the average noise power spectrum (ANPS). The ANPS of the cryogenic accelerometers (2271A) at 8 mK are shown in figure 5, clearly displaying PT harmonics, demonstrating that the accelerometers are sensitive to vibrations at 8 mK. The PT harmonics observed in all three directions also demonstrate that the vibrations transmit to the MC plate both in the vertical and radial directions.

We also performed the noise measurement at the different temperatures by applying a heat load as discussed in Section 2 and letting the temperature equilibrate. Figure 6 shows the ANPS of the accelerometers measured between 15 mK and 1050 mK, illustrating the stability of their performance across this temperature range. Figure 7 similarly demonstrates the time stability of the performance of the accelerometers at 8 mK measured over 5 hours.

We collected two datasets to isolate the vibrational noise contributions from the turbo pump and the air-cooled chiller. The chiller-only data were collected for 2 hours by letting the MC reach base temperature, turning off PTs and turbo pump. Similarly, turbo-only data were collected for 45 minutes by letting the MC reach base temperature, turning off PTs and chiller. Figure 8 shows the chiller-only and turbo-only datasets illustrating that the turbo pump contributes several low frequency noise peaks.

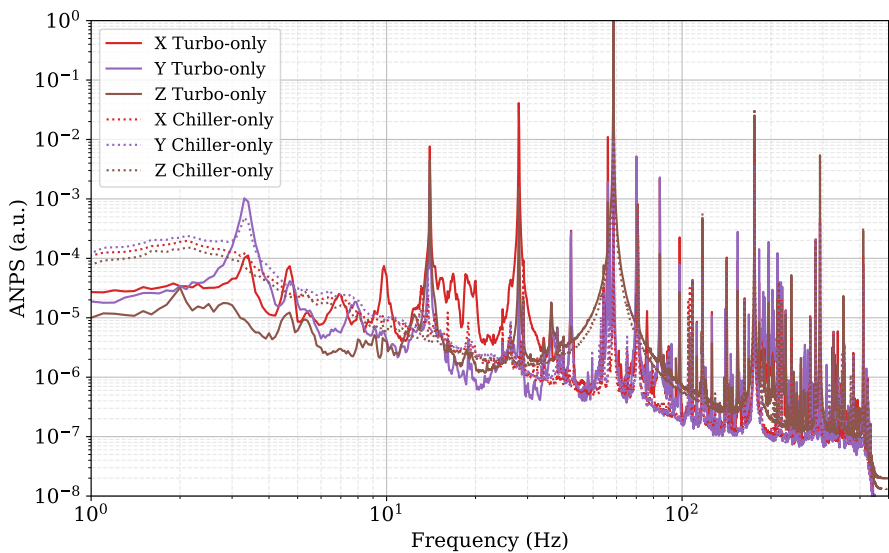


Figure 8. 2271A accelerometer response to cryogenic equipment. Solid lines show data collected when only the turbo pump is on. Dotted lines show data collected when only the air cooled chiller is on. The turbo data collection was kept short to ensure safe vacuum levels for the device operation.

4 Radioassay Results

Measuring the radioactivity of devices installed in close proximity to the experimental volume is crucial for assessing their viability, especially for use in rare event searches. Long-lived radioisotopes such as ^{40}K , ^{238}U and ^{232}Th are of particular concern in low-background experiments. The three accelerometers were assayed at Virginia Tech with a high purity germanium (HPGe) detector for approximately two weeks and the spectrum obtained was compared to a background spectrum (i.e., no sample present) also collected over two weeks. The detector is an Ortec Model GEM30 LLB-GEM-HJ HPGe gamma-ray spectrometer with an integrated cryostat with a relative efficiency of 35%, energy resolution of 1.85 keV FWHM at 1332 keV, and is shielded on all sides

by approximately 10 cm of lead. The detection efficiency for the accelerometer sample geometry was estimated with a GEANT4-based [39] simulation implementing the nominal HPGe detector geometry with the accelerometers approximated as stainless steel cylinders and isotropic sources of ^{238}U , ^{40}K and ^{232}Th confined to the accelerometer volumes.

To validate the simulation, the efficiency was measured with point sources: ^{133}Ba , ^{152}Eu , ^{137}Cs , ^{60}Co and ^{22}Na , which have an activity certified to 5% uncertainty by the vendor [40], and compared to simulations. Between 200 keV and 1410 keV, the ratio of the measured detection efficiency and detection efficiency extracted from simulation was found to be 0.711 ± 0.036 independent of energy. We apply this correction factor to detection efficiencies extracted from the simulation of the accelerometer samples. As a further cross check, a 30.2 g sample of K_2SO_4 powder with activity certified to 1.1% [41] was measured and simulated. The ratio between the measured detection efficiency and that extracted from the simulation was found to be 0.726 ± 0.015 . At 121 keV, we find the measured efficiency is 55% of the efficiency extracted from simulation. At low energy, uncertainty on the detector geometry and possible presence of detector dead layer have a larger impact, and so we apply an additional systematic error on the efficiency below 200 keV.

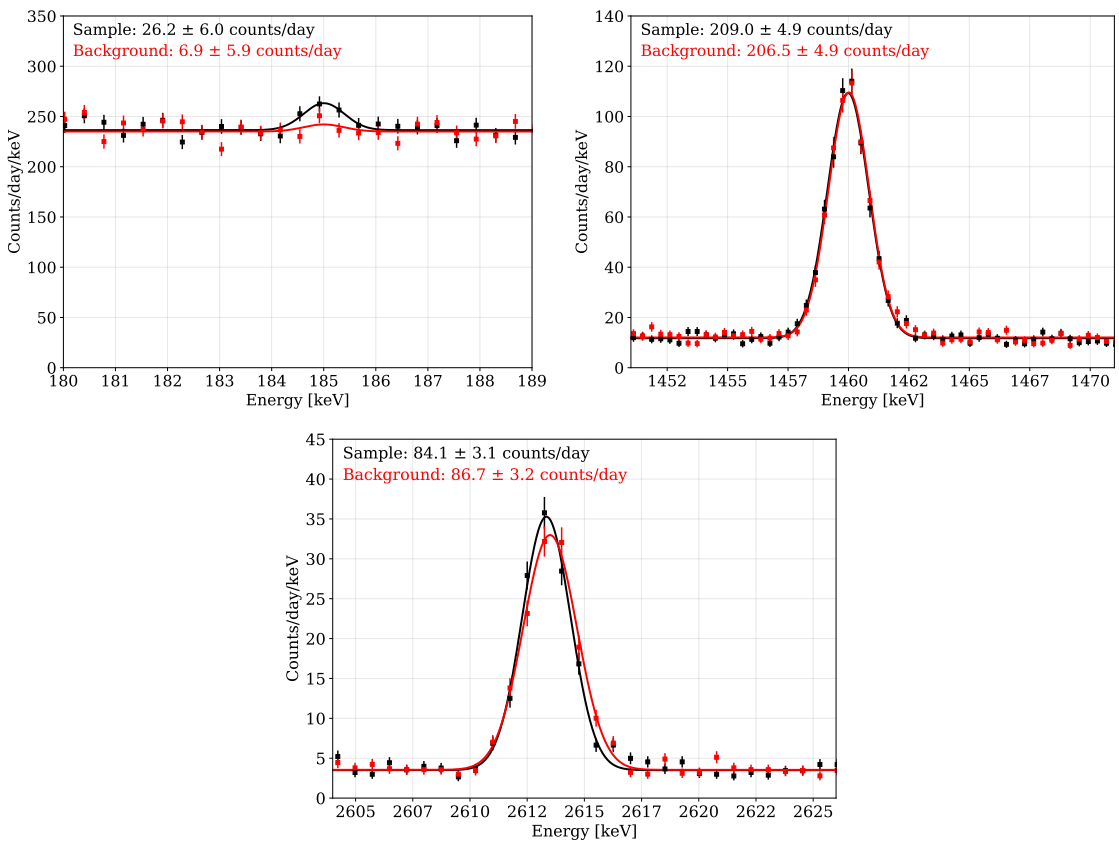


Figure 9. Results of the HPGe counting analysis for the region of interest for ^{226}Ra near 186 keV (top left), ^{40}K near 1460 keV (top right), and ^{208}Tl near 2614 keV (bottom). The black histograms are the data collected with the sample, the red histograms are the data collected with no sample present. The black and red lines are the best-fit models assuming a gaussian gamma-peak and flat background.

Parent	Gamma	Bkg	Sample	Excess	ϵ	Activity
	(keV)	(counts/day)			%	Bq/kg
^{238}U	^{226}Ra (186)	6.9 ± 5.9	26.2 ± 6.0	19.3 ± 8.4	$0.33^{+0.02}_{-0.08}$	0.9 ± 0.4
^{40}K	^{40}K (1461)	206.5 ± 4.9	209.0 ± 4.9	< 13	0.051 ± 0.003	< 3.8
^{232}Th	^{208}Tl (2615)	86.7 ± 3.2	84.1 ± 3.1	< 5.8	0.088 ± 0.004	< 1.0

Table 1. Summary of radioassay results. The reported efficiency, ϵ , is the estimated absolute detection efficiency for the specified gamma ray per decay of the parent source. Upper limits are at 90% C.L., where the integral over the distribution for the excess parameter was restricted to non-negative values. The final column is the estimated specific activity of the specified parent source in the accelerometer samples.

The results of the HPGe counting are summarized in Table 1 and shown in figure 9. The region of interest for each gamma line was modeled with a gaussian peak and flat background to determine the gamma yield with and without sample. We see no evidence of excess counts from ^{40}K or ^{232}Th from the sample. We do observe an excess of counts associated with the ^{238}U chain. We find the gamma yield in the ROI around 186 keV can depend on the range chosen for the fit due to the low peak-to-background ratio in that region. As an alternative, a simple counting between 183 keV and 188 keV yields 1274 ± 10 and 1235 ± 10 counts per day with and without the sample, respectively. If interpreted as due to ^{238}U in the sample at secular equilibrium, this corresponds to an activity of $(2.0 \pm 0.8)\text{Bq/kg}$. The ^{222}Rn background in the counting setup can vary depending on airflow conditions in the lab. Therefore, we rely on the ^{226}Ra line at 186 keV to probe ^{238}U contamination.

5 Discussion

This work demonstrates the use of cryogenic accelerometers to perform vibrational noise measurements at the coldest stage in a DDR across a broad frequency range. It paves the way for various applications, including continuous monitoring of the vibrational environment in DDRs.

The ability to coherently measure noise and assess vibration transmission across different locations opens up a range of applications. As an example, it enables applications such as denoising leveraging continuous, real-time measurements that facilitate ongoing noise assessment and mitigation in vibration-sensitive experiments. As a use case, we consider one of the tri-axial 393B31 accelerometers as the device of interest and the 2271A accelerometers as the *witness* sensors and generate the coherence and transfer function (TF) to characterize the vibration transmission across the various DDR stages.

Following the procedure developed in Ref. [31], we begin by defining the cross-spectral density between any two devices i and j as the time-averaged products of the discrete Fourier transforms (DFT) $\mathcal{F}_i(f)$ and $\mathcal{F}_j(f)$ of their time streams, respectively as

$$G_{i,j}(f) = \frac{2}{T} \langle \mathcal{F}_i^*(f) \cdot \mathcal{F}_j(f) \rangle \quad (5.1)$$

where T is the duration of time windows used for averaging. $G_{i,j}(f)$ is a matrix of size N , where N is the number of DFT bins. The level of correlation between devices for all frequencies can be

quantified using $G_{i,k}$, dropping f , as

$$C_{i,k} = \frac{|G_{i,k}|^2}{G_{i,i}G_{k,k}} \quad (5.2)$$

The TF between device i and device k can then be computed as

$$H_{i,k} = \sum_{j=1}^n G_{i,j}^{-1}G_{j,k}, \quad (5.3)$$

where n is the number of witness sensors. $H_{i,k}$ is a complex $n \times N$ matrix and defines the relationship between device i and device k across all frequencies. Figure 10 shows the coherence and the TF between cryogenic accelerometers and y-aligned room temperature accelerometer.

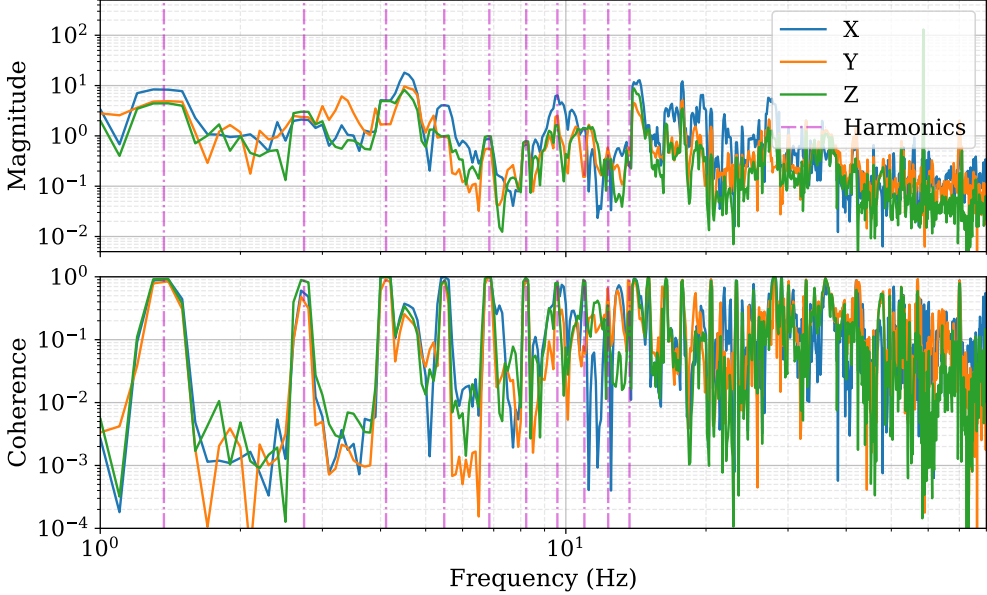


Figure 10. (Top): Transfer function magnitude between 2271A accelerometers in respective directions for 1 hour of data against the 393B31 accelerometer in Y direction. The Y direction was selected as it was the direction with the most sensitivity to PT induced vibrations for the 393B31 accelerometers. (Bottom): Coherence between identical sets of channels as described above.

To use a series of witness sensors i as a way to identify correlations and perform denoising for the data O_k from the sensor k , the TF, $H_{i,k}$, could be used as follows:

$$D_k = O_k - \sum_{i=1}^n H_{i,k}^T A_i \quad (5.4)$$

where D_k is the denoised signal. As long as there are correlations between the witness sensors and the detector, this algorithm performs reasonably well.

This technique was successfully demonstrated [14], and continues to be used, by the CUORE collaboration to denoise their bolometer signals with a series of accelerometers, seismometers,

and antennas acting as witness sensors. Stronger noise correlations between witness sensors and the detector lead to a better denoising performance. For detectors coupled to the lowest stage of a DDR with complex inter-stage couplings—such as CUORE—deploying witness sensors at multiple stages could enhance correlations.

A critical consideration in deploying cryogenic accelerometers in DDRs is the amount of heat they dissipate at mK temperatures. Excessive heat load at this temperature can make it impossible for DDRs to reach their base temperature, and consequently compromise their performance. To estimate the heat load associated with the setups using Endevco 3090C cables and the custom NbTi cables, we used the measured temperature-power curve of the DDR. This curve was obtained previously with no payload attached to MC by applying known heat loads to the resistive heater discussed in Section 2. The power required for the DDR MC to stabilize at 60 mK, the base temperature for the Endevco 3090C cable setup, was calculated in this way to be $119 \mu\text{W}$. The NbTi cable setup, by maintaining the MC base temperature at 8 mK, contributes negligible heat load. For context, the cooling power of the Blue Fors LD400 employed in this work is $15 \mu\text{W}$ at 20 mK. This heat load estimation underscores the need for a careful thermal management when integrating accelerometers into ultra-low temperature cryogenic environments.

In addition to thermal considerations, the intrinsic radioactivity of the accelerometers poses a potential limitation for experiments searching for rare events, such as neutrinoless double beta decay. As discussed in Section 4, HPGe spectroscopy measurements indicate that most γ lines arising from long-lived isotopes of the uranium and thorium decay chains are consistent with ambient background levels, with the one exception being 186 keV γ line associated with ^{226}Ra decay arising from the ^{238}U chain, with a corresponding activity of $(2.0 \pm 0.8)\text{Bq/kg}$. Although the observed activity is not particularly high and remains inconsequential for most cryogenic applications, incorporation of optimized passive shielding might be needed for low background experiments. As part of future investigations, a higher-sensitivity radioassay is being considered at an underground counting facility.

These results represent a critical advancement in vibrational sensing using commercial accelerometers at ultra-low temperatures, yet they highlight the challenges posed by noise in practical deployments. The primary sources of noise stem from electronic interference and environmental signals within the accelerometer-cable assembly, with triboelectric effects emerging as the likely major contributor. While custom NbTi cables were used to minimize heat load, Endevco cables were found to exhibit substantially lower noise at mK temperatures. This indicates that lower noise levels could be achievable beyond what is demonstrated in these results.

Mounting blocks represent another key area for noise reduction enhancement. While copper block was chosen for mounting the 2271A accelerometers, preliminary results using a different cryostat show that anodized aluminum blocks exhibit lower noise drift down to 3 K compared to copper, suggesting a viable alternative. Thus, commercially available anodized aluminum mounting blocks for the 2271A accelerometers will be assessed.

Immediate efforts beyond this work will focus on quantifying noise sources and optimizing cable and mounting configurations. Concurrently, calibration using precision shakers will be explored to establish reliable sensitivity metrics and improve signal-to-noise ratios for real-world applications. Longer term work includes accelerometer placement tests to systematically optimize the vibrational noise detection in complex vibrational environments.

Acknowledgments

This work is supported by the University of Pittsburgh and the US Department of Energy (DOE) Office of Science, Office of Nuclear Physics under Contract under Award No. DE-SC0020423. The authors thank CUORE and CUPID collaborators for productive discussions, technical support, and comments on the paper draft. The authors acknowledge Advanced Research Computing at Virginia Tech for providing computational resources and technical support that have contributed to the results reported within this paper. <https://arc.vt.edu/>.

References

- [1] CUORE collaboration, *CUORE opens the door to tonne-scale cryogenics experiments*, *Prog. Part. Nucl. Phys.* **122** (2022) 103902 [[2108.07883](#)].
- [2] CUPID collaboration, *CUPID, the CUORE upgrade with particle identification*, *Eur. Phys. J. C* **85** (2025) 737 [[2503.02894](#)].
- [3] D. Augu  te et al., *A novel mechanical design of a bolometric array for the CROSS double-beta decay experiment*, *JINST* **19** (2024) P09014 [[2405.18980](#)].
- [4] AMoRE collaboration, *Improved Limit on Neutrinoless Double Beta Decay of Mo100 from AMoRE-I*, *Phys. Rev. Lett.* **134** (2025) 082501 [[2407.05618](#)].
- [5] RICOCHET collaboration, *Ricochet Progress and Status*, *J. Low Temp. Phys.* **212** (2023) 127 [[2111.06745](#)].
- [6] NUCLEUS collaboration, *The ν -cleus experiment: A gram-scale fiducial-volume cryogenic detector for the first detection of coherent neutrino-nucleus scattering*, *Eur. Phys. J. C* **77** (2017) 506 [[1704.04320](#)].
- [7] L. Gastaldo et al., *The electron capture in ^{163}Ho experiment – ECHo*, *Eur. Phys. J. ST* **226** (2017) 1623.
- [8] M. Faverzani et al., *The HOLMES Experiment*, *J. Low Temp. Phys.* **184** (2016) 922.
- [9] SUPERCDMS collaboration, *Projected Sensitivity of the SuperCDMS SNOLAB experiment*, *Phys. Rev. D* **95** (2017) 082002 [[1610.00006](#)].
- [10] CRESST collaboration, *First results from the CRESST-III low-mass dark matter program*, *Phys. Rev. D* **100** (2019) 102002 [[1904.00498](#)].
- [11] EDELWEISS collaboration, *First germanium-based constraints on sub-MeV Dark Matter with the EDELWEISS experiment*, *Phys. Rev. Lett.* **125** (2020) 141301 [[2003.01046](#)].
- [12] C. Enss, ed., *Cryogenic Particle Detection*, vol. 99 of *Topics in Applied Physics*, Springer, Berlin, Germany (2005), [10.1007/b12169](#).
- [13] D. Cousins, S.N. Fisher, A. Gu  nault, R. Haley, I. Miller, G. Pickett et al., *An advanced dilution refrigerator designed for the new lancaster microkelvin facility*, *Journal of low temperature physics* **114** (1999) 547.
- [14] CUORE collaboration, *Constraints on Lepton Number Violation with the 2 tonne-yr CUORE Dataset*, *Science* **390** (2025) 1029 [[2404.04453](#)].
- [15] M.I. Hollister, R.C. Dhuley, C. James and G.L. Tatkowski, *An update on the Colossus mK platform at Fermilab*, *IOP Conf. Ser. Mater. Sci. Eng.* **1302** (2024) 012030.

[16] RICOCHET collaboration, *Characterization of mini-CryoCube detectors from the RICOCHET experiment commissioning at the Institut Laue-Langevin*, *Phys. Rev. D* **112** (2025) 112019 [[2507.22751](#)].

[17] CUORE collaboration, *First-ever detection of microseismic activity with a tonne-scale cryogenic experiment*, [2505.09652](#).

[18] S. Kono, J. Pan, M. Chegnizadeh, X. Wang, A. Youssefi, M. Scigliuzzo et al., *Mechanically induced correlated errors on superconducting qubits with relaxation times exceeding 0.4 ms*, *Nature Commun.* **15** (2024) 3950 [[2305.02591](#)].

[19] C. Lee, H.S. Jo, C.S. Kang, G.B. Kim, I. Kim, S.R. Kim et al., *Vibration isolation system for cryogenic phonon-scintillation calorimeters*, *JINST* **12** (2017) C02057.

[20] A. Wex et al., *Decoupling pulse tube vibrations from a dry dilution refrigerator at milli-Kelvin temperatures*, *JINST* **20** (2025) P05022 [[2501.04471](#)].

[21] M. Kellermann et al., *A Vibration Decoupling System for TES Operation in the COSINUS Dry Dilution Refrigerator*, *J. Low Temp. Phys.* **217** (2024) 418.

[22] CUPID collaboration, *A first test of CUPID prototypal light detectors with NTD-Ge sensors in a pulse-tube cryostat*, *JINST* **18** (2023) P06033 [[2304.04674](#)].

[23] R. Maisonneuve, J. Billard, M. De Jesus, A. Juillard, D. Misiak, E. Olivieri et al., *Vibration decoupling system for massive bolometers in dry cryostats*, *JINST* **13** (2018) T08009 [[1803.03463](#)].

[24] CUORE collaboration, *The CUORE Cryostat: A 1-Ton Scale Setup for Bolometric Detectors*, *J. Low Temp. Phys.* **184** (2016) 590 [[1603.03306](#)].

[25] E. Olivieri, J. Billard, M. De Jesus, A. Juillard and A. Leder, *Vibrations on pulse tube based Dry Dilution Refrigerators for low noise measurements*, *Nucl. Instrum. Meth. A* **858** (2017) 73 [[1703.08957](#)].

[26] A.M.J. van Haan, G.H.C.J. Wijts, F. Galli, O. Usenko, G.J.C. van Baarle, D.J. van der Zalm et al., *Atomic resolution scanning tunneling microscopy in a cryogen free dilution refrigerator at 15 mK*, *Rev. Sci. Instrum.* **85** (2014) 035112 [[1312.6011](#)].

[27] E. Wiens and S. Schiller, *A simple and efficient passive vibration isolation system for large loads in closed-cycle cryostats*, *Review of Scientific Instruments* **92** (2021) 095101.

[28] C. Lee, H.S. Jo, C.S. Kang, G.B. Kim, I. Kim, Y.H. Kim et al., *Vibration Mitigation for a Cryogen-Free Dilution Refrigerator for the AMoRE-Pilot Experiment*, *J. Low Temp. Phys.* **193** (2018) 786.

[29] M. de Wit, G. Welker, K. Heeck, F.M. Buters, H.J. Eerkens, G. Koning et al., *Vibration isolation with high thermal conductance for a cryogen-free dilution refrigerator*, *Rev. Sci. Instrum.* **90** (2019) 015112 [[1810.06847](#)].

[30] D.G. Blair, F.J. van Kann and A.L. Fairhall, *Behaviour of a vibration isolator suitable for use in cryogenic or vacuum environments*, *Measurement Science and Technology* **2** (1991) 846.

[31] K.J. Vetter et al., *Improving the performance of cryogenic calorimeters with nonlinear multivariate noise cancellation algorithms*, *Eur. Phys. J. C* **84** (2024) 243 [[2311.01131](#)].

[32] Endevco Piezoelectric Accelerometer, Model 2271A. <https://wwwpcb.com/products?m=2271a>, 2025.

[33] PCB Piezotronics 4-Channel Dual Mode Signal Conditioner with Charge-to-Voltage Conversion and Voltage Gain, Model 482C64. <https://wwwpcb.com/products?m=482c64>, 2025.

- [34] PCB Piezotronics Piezoelectric Accelerometer, Model 393B31.
<https://wwwpcb.com/products?m=393b31>, 2025.
- [35] PCB Piezotronics 4-Channel Signal Conditioner with Selectable Voltage Gain, Model 482C15.
<https://wwwpcb.com/products?m=482c15>, 2025.
- [36] National Instruments 3-channel 12.8 kS/s C Series DAQ, Model 9230.
<https://wwwni.com/en-us/shop/model/ni-9230.html>, 2025.
- [37] National Instruments compact DAQ Chassis, Model 9178.
<https://wwwni.com/en-us/shop/model/cdaq-9178.html>, 2025.
- [38] Endevco Low Noise Cable Assembly, Model 3090C.
<https://buyendevco.com/cables/3090c-cable-2>, 2025.
- [39] S.A. et al., *Geant4—a simulation toolkit*, *Nuclear Instruments and Methods in Physics Research Section A: Accelerators, Spectrometers, Detectors and Associated Equipment* **506** (2003) 250.
- [40] , “Spectrum Techniques Certificate of Activity.”
<https://wwwspectrumtechniques.com/product/beta-gamma-disk-sources/>, 2022, 15 Feb.
- [41] IAEA, “Certified Reference Material IAEA-RGK-1.”
<https://analytical-reference-materials.iaea.org/iaea-rgk-1>, 2024, 07 March.